Int. J. Therm. Sci. (2001) 40, 649–658

S1290-0729(01)01254-6/FLA

Numerical investigation of forced convection in a plane channel with a built-in triangular prism

Hassen Abbassi [a], Said Turki [a*], Sassi Ben Nasrallah [b]

[a] *Faculté des sciences, Département de physique, Route de Soukra, 3038 Sfax, Tunisie*

[b] *Ecole Nationale d'Ingénieurs, Route de Kairouan, 5000 Monastir, Tunisie*

(Received 19 October 1999, accepted 15 September 2000)

Abstract — Structure of laminar flow and heat transfer, in a two-dimensional horizontal channel differentially heated, with a built-in triangular prism is investigated from the numerical solutions of complete Navier–Stokes and energy equations. The numerical scheme is based on Control Volume Finite-Element Method with the SIMPLER algorithm for pressure-velocity coupling. Many standard test flows are successfully simulated. Results are obtained for Reynolds number ranging from 20 to 250 at $Pr = 0.71$ with constant physical properties. The flow is especially studied in details for two Reynolds numbers, $Re = 30$ as a sample of the symmetric flow, and $Re = 100$ as a sample for the periodic flow. Results are presented to show how the presence of such bluff body affects the flow pattern and the heat transfer from the hot bottom plate to the flow in both cases, symmetric and periodic flows. © 2001 Éditions scientifiques et médicales Elsevier SAS

laminar flow / periodic / obstacle / heat transfer / shedding / vortices / forced convection

Résumé — La convection forcée d'air dans un canal plan différentiellement chauffé et contenant un obstacle ayant la forme d'un prisme triangulaire est étudiée numériquement. Les équations de conservation sont résolues pour une géométrie bidimensionnelle par une méthode de volumes finis à maillage non structuré en conservant la vitesse et la pression comme variables dynamiques du problème. Plusieurs tests de validations du code de calcul ont été réalisés avec succès. Les résultats sont obtenus pour Reynolds allant de 20 à 250 pour $Pr = 0{,}71$. L'écoulement est particulièrement étudié en détails pour $Re = 30$ et $Re = 100$ comme étant deux échantillons respectifs de l'écoulement symétrique et de l'écoulement périodique. L'objectif de ce travail est l'étude de l'effet de l'obstacle sur la structure de l'écoulement et sur les transferts thermiques. © 2001 Éditions scientifiques et médicales Elsevier SAS

ecoulement laminaire / périodique / obstacle / transfert thermique / détachement / tourbillons / convection forcée

Nomenclature

A	length of the triangular prism	m
B	width of the triangular prism	m
c_f	dimensionless skin friction coefficient $= 2(\partial u/\partial y)_w/Re$	
C	$Re c_f$	
C_P	specific heat at constant pressure	$m^2 \cdot s^{-2} \cdot K^{-1}$
f	dominant frequency	s^{-1}
g	gravitational acceleration	$m \cdot s^{-2}$
Gr	Grashof number $= \rho^2 g\beta(T_h - T_c)H^3/\mu^2$	
H	channel width	m
k	thermal conductivity of the fluid	$kg \cdot m \cdot s^{-3} \cdot K^{-1}$
Nu	local Nusselt number $= -(\partial\theta/\partial y)_{y=0}$	
$\overline{Nu}$	space averaged Nusselt number	
$\langle\overline{Nu}\rangle$	space and time-averaged Nusselt number	
P	pressure nondimensionalized by ρu_{max}^2	
Pe	Peclet number $= Re\,Pr$	
Pr	Prandtl number $= \mu C_P/k$	
Ra	Rayleigh number $= Gr\,Pr$	
Re	Reynolds number $= u_{max}B/\nu$	
St	Strouhal number $= fB/u_{max}$	
T	dimensional temperature	K
u_{max}	maximum of u-component at the channel inlet .	$m \cdot s^{-1}$
$\boldsymbol{U}$	velocity vector nondimensionalized by u_{max}	
u, v	velocity components nondimensionalized by u_{max}	
x, y	Cartesian coordinates nondimensionalized by H	

Greek symbols

β	thermal expansion coefficient	K^{-1}
θ	dimensionless temperature $= (T - T_c)/(T_h - T_c)$	
Θ	dimensionless period	

* Correspondence and reprints.

E-mail addresses: Hassen.Abbassi@fss.rnu.tn (H. Abbassi), Said.Turki@fss.rnu.tn (S. Turki), ssbnsrl@ati.tn (S. Ben Nasrallah).

μ	dynamic viscosity of the fluid	$kg{\cdot}m^{-1}{\cdot}s^{-1}$
ν	kinematic viscosity of the fluid	$m^2{\cdot}s^{-1}$
ρ	density of the fluid	$kg{\cdot}m^{-3}$
τ	time nondimensionalized by u_{max}/H	
$\Delta\tau$	dimensionless time step	

Subscripts

c	cold
h	hot
nb	neighboring nodes
av	average
w	wall

1. INTRODUCTION

Flow past bluff bodies between two parallel walls has been investigated by many researchers both numerically and experimentally. This flow situation is popular not only because of its academic attractiveness but also owing to the related technical problems associated with energy conservation and structural design. This type of flow is of relevance for many practical applications, such as electronic cooling and heat exchanger systems. Tropea and Gackstatter [1] investigated experimentally the flow behind a rectangular cylinder placed on the bottom wall of a horizontal channel. The reattachment length is considered as a function of three parameters: Reynolds numbers, blockage ratio and length-to-height ratio, experiments were carried out for Reynolds number in the range $150 < Re < 4\,500$. Davalath and Bayazitoglu [2] carried out a numerical investigation of developing flow over an array of rectangular blocks, representing finite heat sources placed on the bottom of a horizontal channel. The problem represents a mathematical model for integrated circuit components placed on horizontal circuit board. Forced convection in laminar regime and Reynolds number in the range $100 < Re < 1\,500$ were considered. They evaluate the heat flux transferred to the flow and the temperature distribution on the surface of blocks. Biswas et al. [3] presented a numerical study of mixed convection in a symmetrically heated horizontal channel in presence of a square cylinder symmetrically placed in the channel axis. Their study shows that solutions become periodic and a Von Karman vortex street is formed when Reynolds number exceeds the limit value 340. They showed that the thermal buoyancy can perturb the steady wake or attached vortices at the rear of an obstacle and induce transition to periodic flow. A numerical investigation of the wake flow behind an equilateral triangular obstacle was presented by Zielinska and Wesfreid [4]. They showed that the amplitude of self sustained oscillations in the wake has a well defined maximum A_{max} at a certain position X_{max} in the wake. A_{max} diminishes with decreasing Reynolds number and its position X_{max} moves away from the shedding body. This result is confirmed by experiments of Wesfreid et al. [5].

The present work is concerned with the structure of laminar flow and heat transfer in a two dimensional channel differentially heated with a built-in triangular prism. This specifically shaped cylinder is specially used in systems of vortex flowmeters and flame stabilizer in combustion chambers. The investigation is carried out from the numerical solutions of complete Navier–Stokes and energy equations by Control Volume Finite Element Method (CVFEM). After establishing the credibility of the numerical method by comparing with standard test flows, the effects of presence of triangular prism on the flow structure and heat transfer are presented.

2. STATEMENT OF THE PROBLEM

The system of interest is a horizontal plane channel, a triangular prism is symmetrically placed in the channel axis as indicated in *figure 1*. The triangular prism, the top wall and the incoming stream are assumed to be in a constant dimensional temperature T_c, while the bottom wall is at temperature T_h. Computations have been carried out in a channel of dimensionless total length $L/B = 30.75$. The summit of the triangle is located at distance $x_p = 8B$ from the inlet, the aspect ratio of the triangular section is $A/B = 0.5$, the channel width is set to be $H = 4B$. Boundary conditions expressed in dimensionless form are as follows:

$$\text{At } 0 \le x \le L/B;\ y = 0\text{: } u = v = 0,\ \theta = 1,$$

$$\text{At } 0 \le x \le L/B;\ y = 4\text{: } u = v = 0,\ \theta = 0,$$

$$\text{At } x = 0;\ 0 \le y \le 4\text{: } u = y(4-y)/4,\ v = 0,\ \theta = 0,$$

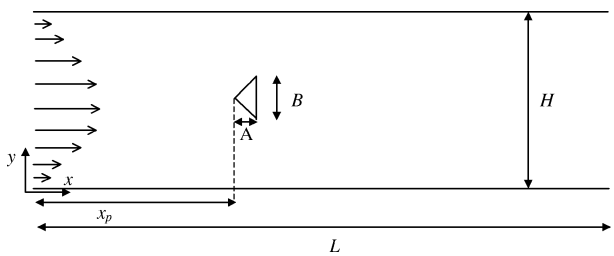

Figure 1. Flow in a horizontal channel with built-in triangular prism.

At $x = L/B;\ 0 \le y \le 4$:

$$\frac{\partial u}{\partial x} = \frac{\partial v}{\partial x} = \frac{\partial \theta}{\partial x} = 0;\ \int_0^4 u\ \mathrm{d}y = 8/3$$

3. GOVERNING EQUATIONS

With reference to Newtonian incompressible fluid of constant physical properties and the Cartesian coordinate system, the dimensionless equations for continuity, momentum, and energy may be expressed in the following conservative form:

$$\mathrm{div}(\boldsymbol{U}) = 0, \tag{1}$$

$$\frac{\partial u}{\partial \tau} + \mathrm{div}(\boldsymbol{Ju}) = -\frac{\partial P}{\partial x}, \quad \boldsymbol{Ju} = u\boldsymbol{U} - \frac{1}{Re}\mathbf{grad}(u), \tag{2}$$

$$\frac{\partial v}{\partial \tau} + \mathrm{div}(\boldsymbol{Jv}) = -\frac{\partial P}{\partial y}, \quad \boldsymbol{Jv} = v\boldsymbol{U} - \frac{1}{Re}\mathbf{grad}(v), \tag{3}$$

$$\frac{\partial \theta}{\partial \tau} + \mathrm{div}(\boldsymbol{J\theta}) = 0, \quad \boldsymbol{J\theta} = \theta\boldsymbol{U} - \frac{1}{Pe}\mathbf{grad}(\theta) \tag{4}$$

In the above equations the space coordinates, velocities, time and pressure are normalized with respectively the width of the triangular prism B, the maximum velocity at the channel inlet $u_{\max}$, the characteristic time $B/u_{\max}$, and the characteristic pressure $\rho u_{\max}^2$. The dimensionless temperature $\theta = (T - T_c)/(T_h - T_c)$ is referred to suitably defined "hot" and "cold" temperatures.

The thermal heat flux transferred from the hot bottom wall to the flow is characterized by the space-averaged Nusselt number evaluated as follows:

$$\overline{Nu} = \frac{1}{L/B}\int_0^{L/B}\left(-\frac{\partial \theta}{\partial y}\right)\mathrm{d}x \tag{5}$$

The space- and time-averaged Nusselt number is defined as:

$$\langle\overline{Nu}\rangle = \left(\frac{1}{\tau_2 - \tau_1}\right)\int_{\tau_1}^{\tau_2}\overline{Nu}\ \mathrm{d}\tau \tag{6}$$

where the time interval $(\tau_2 - \tau_1)$ is the period of oscillation of the space-averaged Nusselt number $\overline{Nu}$.

4. NUMERICAL PROCEDURE

A modified version of Control Volume Finite-Element Method (CVFEM) of Saabas and Baliga [6] is adapted to the standard staggered grid in which pressure and velocity components are stored at different points as indicated in *figure 2(a)*. The control volume is constructed around every node P by joining the centroids of the triangular elements to the midpoints of the sides as indicated in *figure 2(b)* where we have constructed, as example, the control volume corresponding to the u-component. Those of v-component and pressure are obtained by the same manner. Compared to that obtained in classic finite-volume method, the obtained control volume has more faces and brings more neighboring nodes.

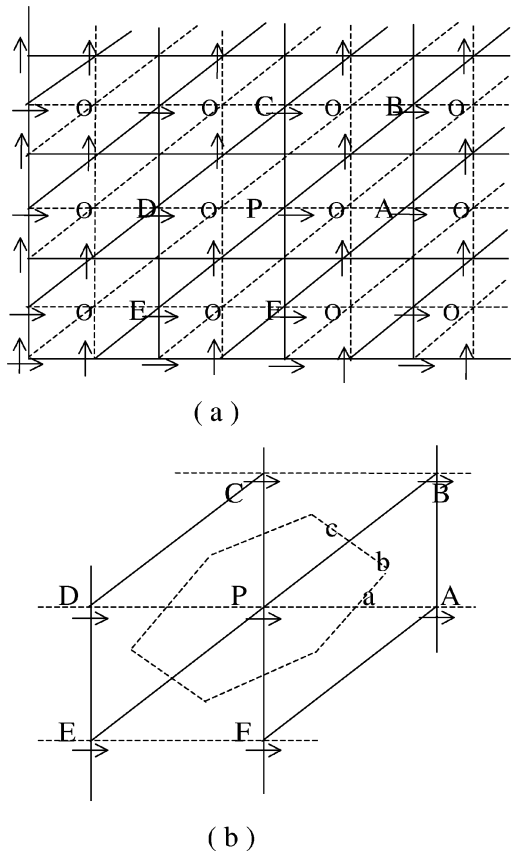

Figure 2. (a) Nodal locations on a staggered grid: O: P nodes, $\rightarrow$: $\boldsymbol{u}$ nodes , $\uparrow$: $\boldsymbol{v}$ nodes (b) Control-volume for u-component.

The conservation equations (2)–(4) are integrated similarly over each of these control volume to obtain equations of nodal values for velocity components and temperature. A special procedure is used to integrate the mass conservation equation (1).

A shape function describing the variation of the dependant variable ϕ $(= u, v \text{ or } \theta)$ is needed to calculate the flux across the control-volume faces. We have follow Saabas and Baliga [6] in assuming a linear and an exponential variations respectively when the dependant variable ϕ is calculated in the diffusive and the convec-

tive terms of the conservation equations. More details and discussions about these functions can be found in references [6–9].

Using the Green–Ostrogradsky theorem, integration of the divergence term in the x-momentum equation (2) over the control-volume surrounding node P gives:

$$\int_{V_\mathrm{p}} \left[\mathrm{div}(\boldsymbol{Ju})\right] \mathrm{d}v = \int_S \boldsymbol{Ju}\cdot\boldsymbol{n}\ \mathrm{d}s \tag{7}$$

where S is the surface area of the control volume V_p surrounding node P, and $\boldsymbol{n}$ is a unit outward normal to the differential surface area $\mathrm{d}s$. Element PAB has two faces ag and gb bounding the control volume around P, the contributions from these two surfaces to the flux of vector $\boldsymbol{Ju}$ in two-dimensional flow can be written as:

$$\int_S \boldsymbol{Ju}\cdot\boldsymbol{n}\ \mathrm{d}s = \int_a^g (Ju_1\cdot n_1 + Ju_2\cdot n_2)\ \mathrm{d}l + \int_g^b (Ju_1\cdot n_1 + Ju_2\cdot n_2)\ \mathrm{d}l \tag{8}$$

where Ju_i and n_i ($i = 1$ or 2) are respectively the components of vectors $\boldsymbol{Ju}$ and $\boldsymbol{n}$. By Simpson's rule we evaluate easily integrals in equation (8). The same treatment of all faces in all elements neighboring the node P must be carried out. The other terms in equation (2) are globally integrated over the entire control-volume around node P [10]. After integration in space, integration in time is necessary. Collecting and simplifying, the discretised x-momentum equation can be written as:

$$A_\mathrm{p}^u u_\mathrm{p} = \sum_{nb} A_{nb}^u u_{nb} + V_\mathrm{p}\left\langle -\frac{\partial P}{\partial x}\right\rangle + \frac{V_\mathrm{p} u_\mathrm{p}^0}{\Delta\tau} \tag{9}$$

where u_p^0 refers to the value of u_p at last time and $\langle -\frac{\partial P}{\partial x}\rangle$is the average value of $(-\frac{\partial P}{\partial x})$ acting over the entire control volume surrounding node P and evaluated by assuming a linear variation of pressure. Equations (3) and (4) for conservation of y-momentum and energy are integrated similarly and written in the same form as equation (9).

$$A_\mathrm{p}^v v_\mathrm{p} = \sum_{nb} A_{nb}^v v_{nb} + V_\mathrm{p}\left\langle -\frac{\partial P}{\partial y}\right\rangle + \frac{V_\mathrm{p} v_\mathrm{p}^0}{\Delta\tau}, \tag{10}$$

$$A_\mathrm{p}^\theta \theta_\mathrm{p} = \sum_{nb} A_{nb}^\theta \theta_{nb} + \frac{V_\mathrm{p}\theta_\mathrm{p}^0}{\Delta\tau} \tag{11}$$

The pressure is indirectly specified through satisfaction of mass conservation equation (1). Equations (9) and (10) can be rewritten as:

$$u_\mathrm{p} = \tilde{u}_\mathrm{p} + B_\mathrm{p}^u\left\langle -\frac{\partial P}{\partial x}\right\rangle, \tag{12}$$

$$v_\mathrm{p} = \tilde{v}_\mathrm{p} + B_\mathrm{p}^v\left\langle -\frac{\partial P}{\partial y}\right\rangle \tag{13}$$

where $\tilde{u}_\mathrm{p}$ and $\tilde{v}_\mathrm{p}$ represents pseudo-velocities components, B_p^u and B_p^v are the pressure-gradient coefficients defined as:

$$\tilde{u}_\mathrm{p} = \frac{\left(\sum_{nb} A_{nb}^u u_{nb} + V_\mathrm{p} u_\mathrm{p}^0/\Delta\tau\right)}{A_\mathrm{p}^u}, \tag{14}$$

$$\tilde{v}_\mathrm{p} = \frac{\left(\sum_{nb} A_{nb}^v v_{nb} + V_\mathrm{p} v_\mathrm{p}^0/\Delta\tau\right)}{A_\mathrm{p}^v}, \tag{15}$$

$$B_\mathrm{p}^u = \frac{V_\mathrm{p}}{A_\mathrm{p}^u}, \tag{16}$$

$$B_\mathrm{p}^v = \frac{V_\mathrm{p}}{A_\mathrm{p}^v} \tag{17}$$

using expressions (14)–(17) pseudo-velocities and pressure-gradient coefficients can be calculated at all nodes of the domain.

The integration of the mass conservation equation (1) over the control volume corresponding to the pressure can be written as:

$$\int_{V_\mathrm{p}} \left(\frac{\partial u}{\partial x} + \frac{\partial v}{\partial y}\right) \mathrm{d}v \cong V_\mathrm{p}\left\{\left\langle\frac{\partial u}{\partial x}\right\rangle + \left\langle\frac{\partial v}{\partial y}\right\rangle\right\} = 0 \tag{18}$$

Where the symbol $\langle\ \rangle$ denotes the average value over the entire control volume. Following Saabas and Baliga [6] and Patankar [11] in assuming a linear variation of u and v components in the treatment of pressure equation, and substituting equations (12) and (13) in equation (18), the mass conservation equation yields to the discretized equation of pressure written in the classic form:

$$A_\mathrm{p}^P P_\mathrm{p} = \sum_{nb} A_{nb}^P P_\mathrm{p} + b^P \tag{19}$$

where b^P is the source term arising from pseudo-velocity fields.

The SIMPLER algorithm was applied to resolve the pressure-velocity coupling in conjunction with an Alternating Direction Implicit (ADI) scheme for performing the time evolution.

5. VALIDATION

Several standard test flows are successfully simulated. Comparisons with benchmark solutions and experimental measurements are shown in this section for three test problems: Poiseuille–Benard channel flow, laminar flow over a backward-facing step and flow in a horizontal channel with a built-in square cylinder.

5.1. Poiseuille–Benard channel flow at $Re = 10$, $Pe = 20/3$ and $Ra = 10^4$

This channel flow would be a simple Poiseuille flow if there were no heating from below and Benard flow (at Rayleigh number $Ra = 10^4$) if the ends were closed. Governing equations are adimensionnalized by the average velocity at the inlet and the channel width. To take into account the effect of thermal buoyancy we must add the term $[\theta Ra/(Pe\,Re)]$ to the second member of the equation (3). In the present test problem our results are compared to those reported by Sani and Gresho [12], Comini et al. [13] and Evans and Paolucci [14]. At the channel inlet, a fully developed parabolic profile for the axial velocity is deployed. No-slip boundary conditions for velocities on all solid walls are used. The bottom and the top walls are maintained respectively at hot and cold temperature. At the inlet, a linear variation of temperature is imposed. At the exit and as in references [12–14], a convective boundary condition is applied for all dependent variables.

The flow is supposed to be laminar and two-dimensional. The study of grid dependence indicated in *table I* shows that a uniform grid of 140×15 is sufficient to obtain accurate results.

Figure 3 presents streamlines at the instant when a minimum is reached in the temperature at the midpoint of the section exit. This figure is analogue to that reported in reference [12]. More quantitative comparisons concerning the period Θ and the space- and time-averaged Nusselt number $\langle\overline{Nu}\rangle$ are reported in *table II*. These results demonstrate good accuracy and competence of our numerical code. Especially our results are close to that reported by Evans and Paolucci [14], where the errors in the period and in the space- and time-averaged Nusselt number are respectively 4.7% and 0.87%. It must be pointed out that results reported in *table II* are referred to a domain two times longer than that indicated in *figure 3*.

TABLE I
Grid dependence.

Grid	101×11	140×15	161×17
$\langle\overline{Nu}\rangle$	2.360	2.402	2.412
Number of cells	11	12	12

TABLE II
Poiseuille–Benard channel flow: $Re = 10$, $Pe = 20/3$ and $Ra = 10^4$.

Reference	Present	Comini [13]	Evans [14]
Period Θ	1.395	1.273	1.332
$\langle\overline{Nu}\rangle$	2.536	2.574	2.558

5.2. Laminar flow over a backward-facing step

The geometry and boundary conditions for this flow are shown in *figure 4*. The flow is considered to be laminar and two-dimensional. The study of grid dependence is performed at $Re = 400$ for three non uniform grids. 48×11, 69×21 and 106×31. Results shows that, when we pass from a grid of 48×11 to 69×21 and after to 106×21, the reattachment length undergoes an increase of respectively 8.8% and 0.5%. Then a grid of 69×21 is retained. As defined by Armaly et al. [15], the Reynolds number is based on the bulk velocity at the inlet boundary and the hydraulic diameter. Reynolds numbers in the range $100 \leq Re \leq 800$ are considered here. In *figure 5*, numerical results of reattachment length for different Reynolds numbers are shown in comparison with the experimental and computational results of Armaly et al. [15] and Kim and Moin [16]. The dependence of the reattachment length on Reynolds numbers is

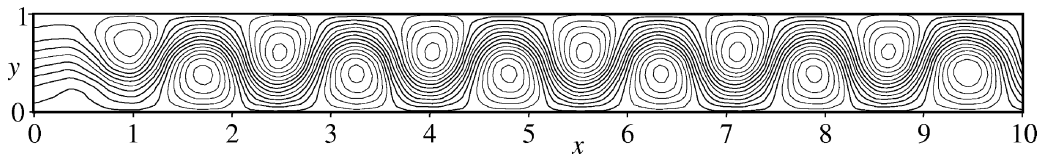

Figure 3. Poiseuille–Benard flow: Streamlines.

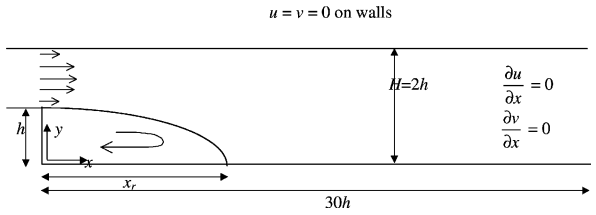

Figure 4. Flow over a backward-facing step (1 : 2 expansion ratio).

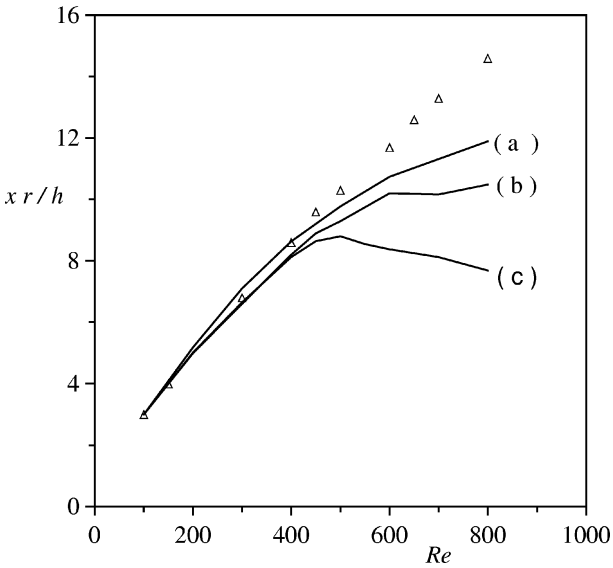

Figure 5. Reattachment length as a function of Reynolds number: Δ: Data from Armaly et al. [15]: (a): Computation of Kim and Moin [16] (grid: 101×101); (b): Present results (69×21); (c): Computation of Armaly et al. [15] (45×45).

in good agreement with the experimental data for *Re* up to about 500, the error is less than 4.5% for *Re* less than 400 and less than 9.7% for *Re* up to 500. From $Re = 600$ computed results start to deviate from the experimental values. It is most likely, as Armaly et al. [15], Kim and Moin [16] and Sohn [17] have pointed out that the difference may have come from three-dimensional effects of the experiments. In *figure 6*, we present the numerical u-velocity distribution for $Re = 389$ at different channel sections, compared to the experimental measurements of Armaly et al. [15]. These figures show that the comparison is very good at all sections.

5.3. Flow in a horizontal channel with a built-in square cylinder

This configuration was investigated numerically and experimentally by Davis et al. [18] and numerically

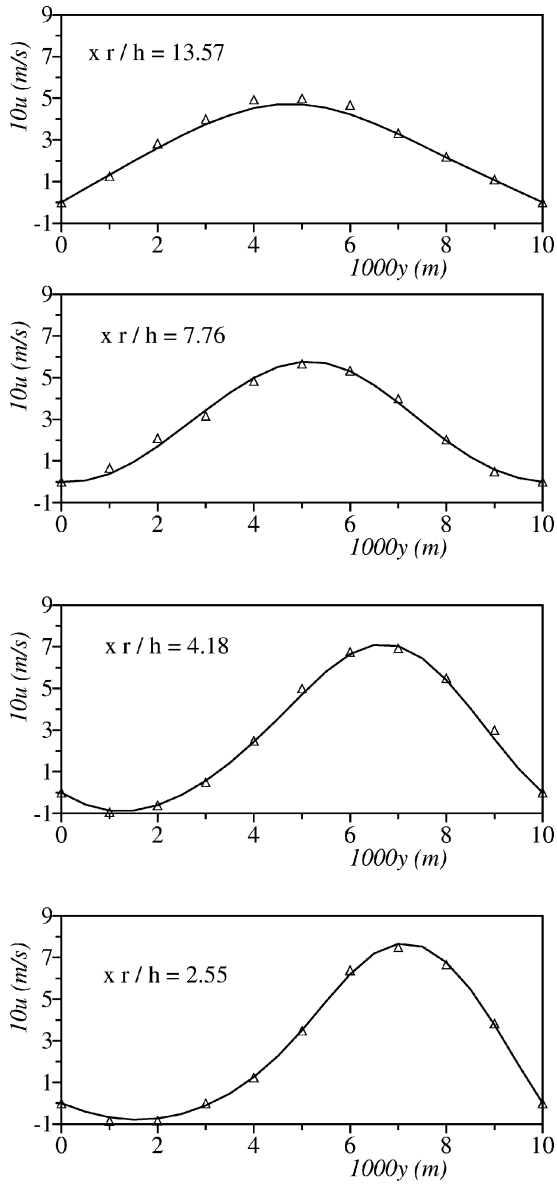

Figure 6. u-velocity distribution at various locations for backward facing step. —: Present calculation; Δ: Data from Armaly et al. [15].

by Biswas et al. [3]. In this study, we compare our values of Reynolds and Strouhal numbers, characterizing respectively the onset and the frequency of vortex shedding, with those of Davis et al. [18] and Biswas et al. [3]. The square cylinder is symmetrically placed in the channel axis. The Reynolds number is as defined in the nomenclature, *B* represents now the width of the square cylinder. All results presented are obtained using a non uniform 105×21 grid. The use of

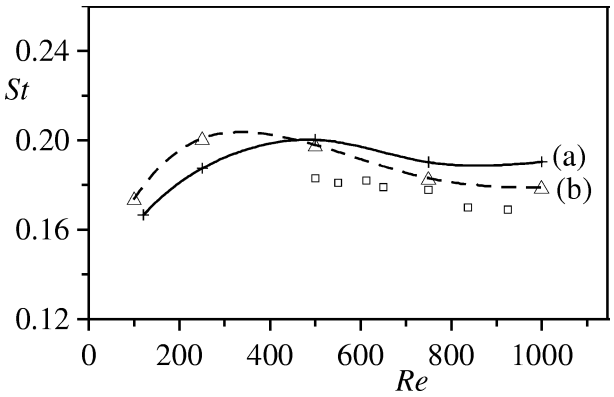

Figure 7. Strouhal numbers versus Reynolds numbers: (a): Present results(105×21); (b): Numerical results of Davis et al. [18] (76×42); □: Experiment of Davis et al. [18].

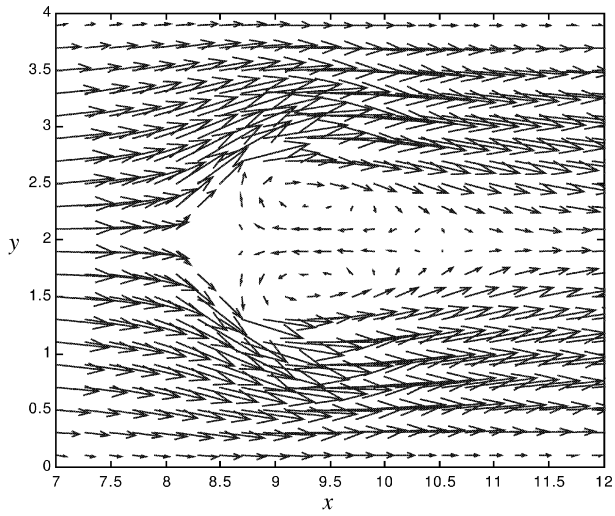

Figure 8. Velocity field for $Re = 30$.

a more refined grid 131×32 lead to an increase of the Strouhal number of only 3.4% (for $Re = 500$) without any remarkable change in the global structure of the flow.

The computational results of the present study show that the onset of vortex shedding was observed at a Reynolds number in the vicinity of 115. Davis et al. [18] observed periodicity in computations at $Re = 100$. However they employed experimentally obtained velocity profiles at the channel inlet instead of the parabolic profile that we use. This periodicity was observed by Biswas et al. [3] at $Re = 340$, but their Reynolds number is based on the average velocity at the inlet and on the channel width H. When converted to a Reynolds number as defined above this value will be $Re = 127$. *Figure 7* summarizes the variation of Strouhal numbers with Reynolds numbers. As can be seen, results obtained are in good agreement with those reported by Davis et al. [18]. The maximum error committed is less than 6.7% by report to numerical values and less than 11.7% in comparison with experimental measurements.

6. RESULTS AND DISCUSSION

After verifying that the implemented numerical code gives accurate results for laminar two dimensional flows between two parallel plates, a solution for the flow described in *figure 1* was next sought. Grid refinement tests have been performed for the case $Re = 100$ using three non uniform grids 72×13, 105×21 and 131×32. Results shows that when we pass from a grid of 105×21 to a grid of 131×32 the space- and time-averaged Nusselt number $\langle\overline{Nu}\rangle$ and the Strouhal number *St* undergoes an increase of only 4.2% and 2.8% respectively, then, for reasons of calculation coast, the grid of 105×21 is retained ($0.18 \leq \Delta x \leq 0.6$, $\Delta y = 0.2$) with a time step $\Delta\tau = 0.01$. In all this study the structure of the flow fields is specified with the help of velocity vector plots and confirmed by the behavior of a signal trace of velocity in the wake. It should be noted that for the periodic flow all solutions are dependent on the time, then, in the following study curves and velocity fields are given at an arbitrary instant.

Solutions are first obtained for $Re = 30$. For this relatively low Reynolds number, the convergence of the numerical procedure is easily obtained. Solutions converge quickly to their asymptotic values. The velocity profiles at different axial locations in the channel are symmetrical about the channel axis. Two symmetrical vortices appear behind the triangular prism on each side of the wake turning in place in opposite sense (*figure 8*).

A series of computations were carried out, by increasing slowly the Reynolds number to determine the critical Reynolds number separating the symmetric and periodic flows. At $Re = 45$ the wake loses its original symmetry. Oscillations in the wake grow in magnitude, and it begins to shed vortices into the stream. The flow in the wake becomes periodic. As in references [18, 19], the destabilization of the flow happens without any need of imposing external perturbations, the action of small truncation errors and computer's round-off errors were sufficient to initiate vortex shedding. *Figure 9* shows a typical vortex street behind the triangular prism for $Re = 100$.

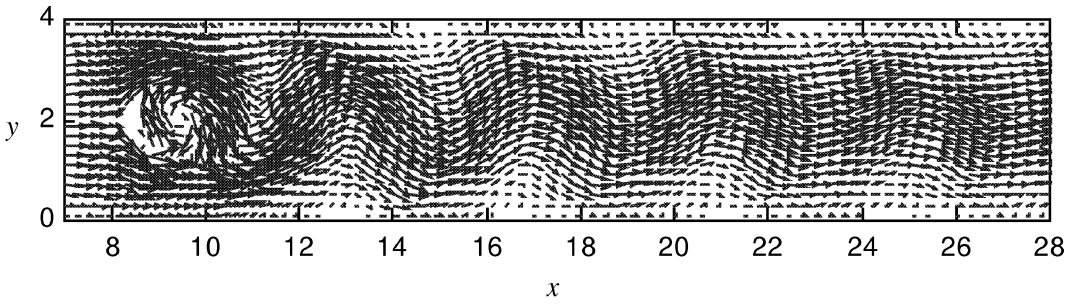

Figure 9. Velocity field for $Re = 100$.

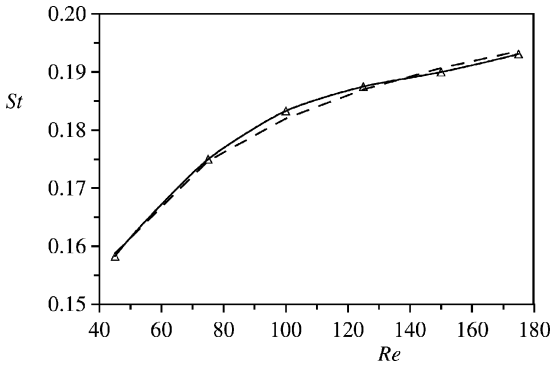

Figure 10. Strouhal numbers versus Reynolds numbers. Solid line: Present study; Dashed line: Empirical law of Fey et al. [22].

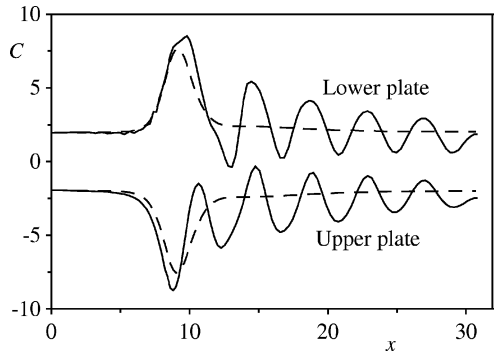

Figure 11. Variation of skin friction on the channel walls. Dashed line: $Re = 30$; Solid line: $Re = 100$.

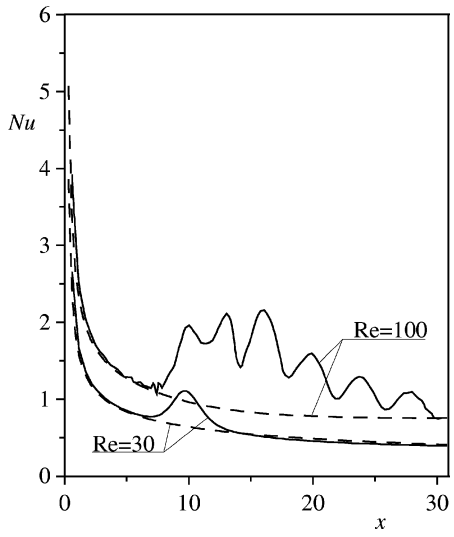

Figure 12. Local Nusselt number distribution along the lower wall. Solid line: flow with triangular prism; Dashed: flow without triangular prism.

Jackson [20] report a critical Reynolds number of 31 from numerical investigation of flow around a triangular prism of the same geometry as ours but placed in an infinite medium (0% blockage). We estimate that this difference in Re_c is due to the presence of an important blockage (25%) in our configuration. As mentioned by Sohankar et al. [21], it may be conjectured that the critical Reynolds number characterizing the onset of vortex shedding increases with increasing blockage. Zielinska et Wesfreid [4] found a critical Reynolds number of 38.3 from their numerical simulation of wake flow behind an equilateral triangular obstacle (then, aspect ratio $= 0.87$) with a blockage of 6.66%. The critical value $Re_c = 45$ is far less then the value correspondent to a square cylinder placed in the same flow as the present triangular cylinder ($Re_c = 115$: present work, see Section 5.3). This comparison lead to the conclusion that Re_c depends strongly on the geometry of the bluff-body.

Recently, Fey et al. [22], based on their experiments, propose a new law for the vortex shedding from a circular cylinder which describes the Strouhal–Reynolds number dependency as: $St = a + b/\sqrt{Re}$ (Re is based on the diameter of the cylinder and the incoming velocity). In the range $47 < Re < 180$, coefficients are $a = 0.2684$ and $b = -1.0356$. For the triangular prism, this law is also

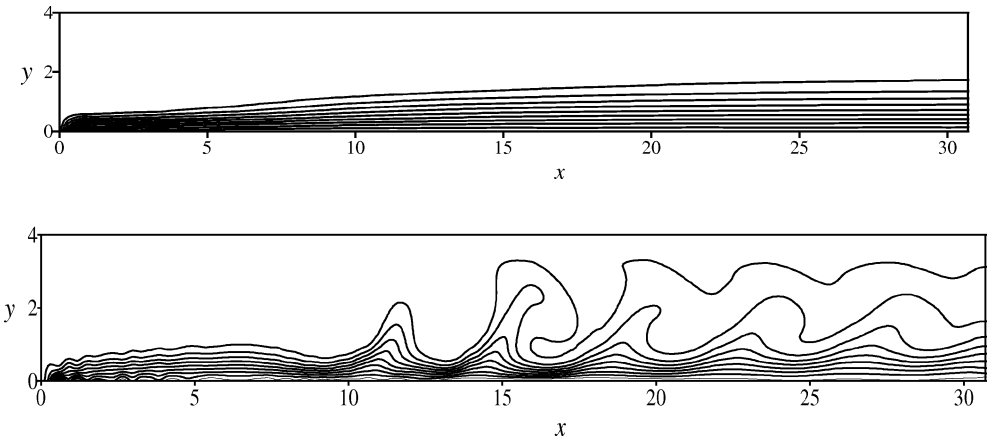

Figure 13. Isotherms at $Re = 100$ respectively without and with triangular prism from 1 (at the bottom wall) to 0 (at the top wall) by interval 0.1.

in good agreement with numerical results as indicated in *figure 10*, but coefficients are different and takes the values $a = 0.2294$ and $b = -0.4736$. Comparing the coefficients b we deduce that the Strouhal number varies more quickly with Reynolds number for the circular cylinder placed in an infinite media than for triangular prism placed between two parallel plates.

The local skin friction coefficient C ($C = Re\, c_f$) is presented in *figure 11*. At $Re = 30$ (symmetric flow), the coefficient C for the two walls is symmetric about the value $C = 0$. This result is expected because the symmetrical flow behaves by the same manner near the two plates. The local coefficient C, on both walls increase (in absolute value) to a peak located behind the triangular prism, due to the acceleration of the flow, and thereafter decreases, due to deceleration, and tends toward their asymptotic values in fully developed flow. At $Re = 100$ (periodic flow), a complete change of the behavior of C is observed. Curves become instantaneously waved along the two walls behind the triangular prism with decrease amplitude when we move away from the prism. We have verified for many Reynolds numbers and at different instants that the maximums (in absolute value) of the local coefficient C coincides always with tops of the Von Karman street.

In the following study our attention will be focused on the effect of the presence of the triangular prism on the heat transferred from the hot wall to the flow. *Figure 12* is a plot of the local Nusselt number along the hot plate. At $Re = 30$, the presence of triangular prism has just a little local effect by increasing slowly the local Nusselt number. In contrast, at $Re = 100$ the effect of the presence of the triangular prism is more

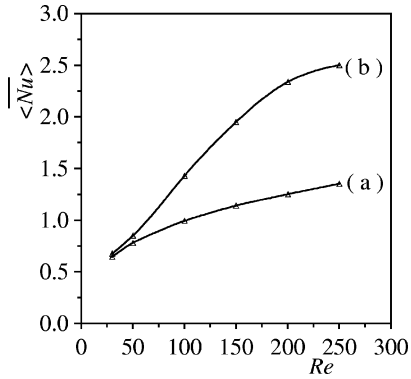

Figure 14. Variation of the space- and time-averaged Nusselt numbers with Reynolds numbers. Upper curve: Flow with triangular prism; Lower curve: Flow without triangular prism.

important, the solid line is well disturbed, but appears floating above the dashed line. An immediate conclusion can be made: the periodic flow leads to favour the heat transfer from the hot plate to the near flow, this heat is immediately transported by the Von Karmen street to the medium flow. This conclusion is confirmed in *figures 13* where we present the isotherms in presence and absence of the obstacle at $Re = 100$. The thermal boundary layer in presence of the triangular prism is well disturbed by the periodic flow, especially isotherms 0.1 and 0.2 are removed far away and tend to be convected toward the top plate proving hence that the medium flow is more heated in periodic flow than in symmetric flow.

Figure 14 summarizes the variation of the space- and time-averaged Nusselt numbers with Reynolds numbers. At relatively low Reynolds numbers corresponding to the

symmetric and the beginning of periodic flows ($Re \leq 50$) the presence of the triangular prism has no significant effect in the space- and time-averaged Nusselt number $\langle \overline{Nu} \rangle$. Increasing Reynolds number, curves start to separate, the presence of the triangular prism leads to an important increase of the space- and time-averaged Nusselt number compared with that obtained without prism. At $Re = 250$ this augmentation is about 85%.

7. CONCLUSION

A numerical investigation from direct solutions of complete Navier–Stokes and energy equations of two-dimensional forced convection of air in a horizontal channel differentially heated with a built-in triangular prism was presented. The numerical scheme is based on Control Volume Finite Element Method adapted to the standard staggered grid with the SIMPLER algorithm and the ADI procedure. According to the validation the obtained numerical code gives accurate solutions.

For the studied configuration shown in *figure 1*, results are summarized as follows: (1) the transition from symmetric flow to periodic flow is observed at Reynolds number in the vicinity of 45. (2) The Strouhal number of the periodic flow behaves as: $St = 0.2294–0.4736/\sqrt{Re}$. (3) For the symmetric flow ($Re < 45$) the presence of the triangular prism has only a local weak effects on the heat transfer and on the flow pattern, while, in periodic flow ($Re \geq 45$), heat transfer is seen to increase strongly with Reynolds number in presence of the triangular prism. An augmentation of about 85% in the space- and time-averaged Nusselt number is recorded at $Re = 250$. This result can be of interest in engineering.

REFERENCES

[1] Tropea C.D., Gackstatter R., The flow over two-dimensional surface-mounted obstacles at low Reynolds numbers, J. Fluids Engrg. 107 (1985) 489–494.

[2] Davalath J., Bayazitoglu Y., Forced convection cooling across rectangular blocks, J. Heat Transfer 109 (1987) 321–328.

[3] Biswas G., Laschefski H., Mitra N.K., Fiebig M., Numerical investigation of mixed convection heat transfer in a horizontal channel with a built-in square cylinder, Numer. Heat Transfer Part A 18 (1990) 173–188.

[4] Zielinska B.J., Wesfreid J.E., On the spatial structure of global modes in wake flow, Phys. Fluids 7 (1995) 1418–1424.

[5] Wesfreid J.E., Goujon-Durand S., Zielinska B.J.A., Global mode behavior of the streamwise velocity in wakes, J. Phys. II 6 (1996) 1343–1357.

[6] Saabas H.J., Baliga B.R., Co-located equal-order control-volume finite-element method for multidimensional, incompressible, fluid flow part I: formulation, Numer. Heat Transfer Part B 26 (1994) 381–407.

[7] Prakash C., An improved control volume finite-element method for heat and mass transfer, Numer. Heat Transfer 9 (1986) 253–276.

[8] Hookey N.A., A CVFEM for two-dimensional viscous compressible fluid flow, Ph.D. thesis, Dept. of Mech. Engrg., McGill University, Montreal, Quebec, 1989.

[9] Elkaim D., Reggio M., Camarero R., Numerical solution of reactive laminar flow by a control-volume based finite-element method and the vorticity-stream function formulation, Numer. Heat Transfer Part B 20 (1991) 223–240.

[10] Volker S., Burton T., Vanka S.P., Finite-volume multigrid calculation of naturel convection flows on unstructed grids, Numer. Heat Transfer Part B 30 (1996) 1–22.

[11] Patankar S.V., Numerical Heat Transfer and Fluid Flow, Ser. Comp. Meth. in Mech. and Therm. Sci., McGraw-Hill, New York, 1980.

[12] Sani R.L., Gresho P.M., Résumé and remarks on the open boundary condition minisymposium, Internat. J. Numer. Meth. Fluids 18 (1994) 983–1008.

[13] Comini G., Manzan M., Cortella G., Open boundary conditions for the streamfunction of unsteady laminar convection, Numer. Heat Transfer Part B 31 (1997) 217–234.

[14] Evans G., Paolucci S., The thermoconvective instability of plane Poiseuille flow heated from below: A benchmark solution for open boundary flow, Internat. J. Numer. Meth. Fluids 11 (1990) 1001–1013.

[15] Armaly B.F., Durst F., Pereira C.F., Experimental and theoretical investigation of backward-facing step flow, J. Fluid Mech. 127 (1983) 473–496.

[16] Kim J., Moin, Application of fractional-step method to incompressible Navier–Stokes equations, J. Comput. Phys. 59 (1985) 308–323.

[17] Sohn J.L., Evaluation of fidap on some classical laminar and turbulent benchmarks, Internat. J. Numer. Methods Fluids 8 (1988) 1469–1490.

[18] Davis R.W., Moore E.F., Purtell L.P., A numerical-experimental study of confined flow around rectangular cylinders, Phys. Fluid 27 (1984) 46–59.

[19] Persillon H., Braza M., Physical analysis of the transition to turbulence in the wake of a circular cylinder by three-dimensional Navier–Stokes simulation, J. Fluid Mech. 365 (1998) 23–88.

[20] Jackson C.P., A finite-element study of the onset of vortex shedding in flow past variously shaped bodies, J. Fluid Mech. 182 (1987) 23–45.

[21] Sohankar A., Norberg C., Davidson L., Low–Reynolds-number flow around a square cylinder at incidence: study of blockage, onset of vortex shedding and outlet boundary condition, Internat. J. Numer. Meth. Fluids 26 (1998) 39–56.

[22] Fey U., Konig M., Eckelmann H., A new Strouhal–Reynolds-number relationship for the circular cylinder in the range $47 < Re < 2{\cdot}10^5$, Phys. Fluids 10 (1998) 1547–1549.